Computers and Geotechnics 69 (2015) 396–410
Please find the formal publication on ScienceDirect via:
http://dx.doi.org/10.1016/j.compgeo.2015.06.003

Coupled modeling of Excavation Damaged Zone in Boom clay: Strain Localization in rock and distribution of Contact Pressure on the gallery's lining

F. Salehnia[a,*], F. Collin[a], X.L. Li[b], A. Dizier[b], X. Sillen[b,1], R. Charlier[a]

[a] *Université de Liège (ULg), Département ArGEnCo, Chemin des Chevreuils, 1, 4000 Liège, Belgium*
[b] *European Underground Research Infrastructure for Disposal of Nuclear Waste in Clay Environment (EIG EURIDICE), 2400 Mol, Belgium*

Abstract

Around galleries excavated at depth in geological media, the creation of a damaged zone with significant irreversible deformation is generally unavoidable. In the case of a geological disposal system for high-level radioactive waste, the resulting change in the host rock properties in this damaged zone may potentially be important with respect to the long-term evolution and the performance of that system. In this context, predicting the extent of the so-called Excavation Damaged Zone (EDZ) and, possibly, the fractures' network topology remains a challenge. This study is aimed to simulate numerically the extension of this zone at the large scale's excavation, around the Connecting gallery (HADES URL, Mol, Belgium), in Boom clay host rock through analyzing the evolution of strain localization in shear bands mode. To realistically model the involved phenomena, the concrete lining is considered on the gallery wall highlighting its impacts on the evolution of convergence and EDZ around the gallery. The focus of the current paper is made on analyzing the coupled hydro-mechanical behavior of Boom clay host rock during and after the gallery excavation with respect to the evolution of localized shear bands around the gallery. This study is accompanied by the analysis of the contact mechanism on the interface between the clay massive and the lining. The obtained results reveal some interesting features regarding the contact phenomenon relatively to the evolution pattern of shear bands within the clay around the gallery. To assess the reliability of the proposed approach, a discussion on some in-situ observations during the gallery's construction is also performed based on which a good agreement is found between the in-situ evidence and simulated results.

Keywords: Boom clay, Connecting gallery, Strain localization modeling, Lining, Contact pressure, Pore water pressure evolution

1. Introduction

In all countries equipped with nuclear power plants, the production of highly radioactive waste is an unavoidable outcome of the contribution of this energy to the global electricity generation. In the framework of the long-term management of these high-level nuclear wastes, storing them in deep stable geological formations is generally considered as a possible solution. Geological disposal facilities (GDFs) combine a suitable system of engineered barriers with an host rock with favorable confinement properties at a depth that ensures adequate isolation from man and the environment. These facilities are regarded by some as an acceptable solution [1]. A very low hydraulic conductivity is one of the desirable properties for candidate host rocks [2] which ensures a limited radionuclide transport rates in the event that a loss of containment occurs due to the degradation of the engineered barrier system.

The underground excavation process is expected to induce stress redistribution within a perturbed zone around the openings which leads to trigger the damage propagation. A zone with the significant irreversible deformations and important modifications in the hydro-mechanical and geo-chemical host rock's properties is expected to be created resulting to the macro and micro-fracturing and a rearrangement of rock structures. This zone is called as Excavation Damaged Zone (EDZ) [3]. In fact, as the rock is damaged, crack networks are created. They could then constitute preferential flow paths depending on the network connectivity and conse-

*Corresponding author. Tel: +32 4 366 3790
Email address: f.salehnia@ulg.ac.be (F. Salehnia)
[1] Present address: Belgian Agency for Nuclear Waste and Fissile Materials (ONDRAF/NIRAS), Avenue des arts 14, 1210 Brussels, Belgium

quently, they could alter the favorable original flow and transport properties of the rock masses. This issue is of a paramount importance in the context of long-term management of the high-lived and high-level nuclear waste disposal. Thence, the simulation of fracturing structure and extension of this zone at the large scale's excavation is the basic objective of this study.

Clay formations are considered to be well-suited for hosting radioactive waste repositories in a number of European countries [4], because of their natural advantageous properties among which there is a very low hydraulic conductivity. Boom clay is a plastic clay located in the north of Belgium. Boom clay formation is being studied as an candidate for this purpose considering its low hydraulic conductivity [2] and important self-sealing capacities (sealing is defined as the reduction of fracture permeability by any of hydro-mechanical, hydro-chemical, or hydro-biochemical processes [5]).

The localized shear bands are commonly observed as a phenomenon leading up to failure in geomaterials, in the laboratory tests or in the fields [6, 7, 8]. During the construction of Connecting gallery in Boom clay host rock, the shear induced fractures were observed [9]. Indeed, this type of fracturing, or discontinuities as often called, are frequently preceded by development of the localization of strains in narrow so-called shear bands. Therefore, in a progressive failure, these shear zones with localized plastic strain are realistically giving rise to the discontinuities, the rupture zones. Hence, to better understand the mechanisms leading to this fractures' network, we propose to analyze the EDZ and its extension around the Connecting Gallery, during its construction and in the long-term, by numerical modeling, in the framework of a strain localization approach in shear band mode. As a consequence, the shear bands with finite thickness are modeled, within the theory of continuum mechanics, to simulate the probable surface of the localized failure and discontinuities. Another approach can be modeling explicitly the ruptured zone with discontinuities in displacements. The latter was the subject of some early studies in order to model the strain localization induced by tunneling [10, 11].

Using a regularization method to properly model the strain localization phenomenon, the hydro-mechanical processes are analyzed in interaction with the evolution of localized shear bands. The coupled hydro-mechanical behavior of Boom clay is studied through the finite element simulation applying an elasto-plastic constitutive model including strain hardening/softening. Over the past decades, many experimental investigations have been conducted to understand the mechanism of localized failure in geomaterials [7] from which one of the essential factors affecting the process can be the anisotropy of material [12]. So the material cross-anisotropy is also considered in our numerical computation.

The concrete lining has an essential role in case of the deep excavation of the underground galleries in the plastic Boom clay. Indeed, it could highly decrease the extent of damaged zone and the convergence around the gallery. Hence, studying the contact mechanism on the interface between the clay mass and the lining around the gallery's opening is also aimed in this paper. In fact, during the excavation, the clay mass converges towards the lining which is followed by the generation of some contact pressure on the interface between two bodies upon contact. The physical relation between this contact phenomenon and the onset of localized shear bands in Boom clay mass is discussed in this study as an open issue of particular interest.

2. Theoretical framework

Taking into account a deformable two-phase medium (i.e., solid and water) where the mass transfers occurs [13, 14], the finite element method has been chosen to simulate the hydro-mechanical process governing the phenomena. The finite element code LAGAMINE, developed at Université de Liège is used in our study [15, 16]. Interested readers are referred to [14] for a detailed finite element framework incorporated into the LAGAMINE code.

2.1. Elasto-plastic constitutive model

The Drucker-Prager yield limit [17] in the framework of a frictional elasto-plastic model is used as the constitutive mechanical law for the rock (compressive stress are taken as positive):

$$F \equiv II_{\hat{\sigma}} - m\left(I_\sigma + \frac{3c}{\tan\phi_c}\right) = 0, \tag{1}$$

where $I_\sigma = \sigma_{ij}\delta_{ij}$ is the first stress invariant, $II_{\hat{\sigma}}$ is the second deviatoric stress invariant defined by Eq. (2) in which $\hat{\sigma}_{ij}$ is the deviatoric stress tensor, m is given as Eq. (3), c is the cohesion, and ϕ_c is the compression friction angle.

$$II_{\hat{\sigma}} \equiv \sqrt{\frac{1}{2}\hat{\sigma}_{ij}\hat{\sigma}_{ij}}; \quad \hat{\sigma}_{ij} = \sigma_{ij} - \frac{I_\sigma}{3}\delta_{ij}, \tag{2}$$

$$m = \frac{2\sin\phi_c}{\sqrt{3}\,(3 - \sin\phi_c)}, \tag{3}$$

In order to introduce the plastic cross-anisotropy of the material in our modeling, the cohesion is defined depending on the angle between major principle stress and the normal to the bedding plane (Eq. (4)) [12]. The behavior is considered to be isotropic in the plane of bedding and the direction of anisotropy is perpendicular to the bedding.

$$c_{0\,or\,f} = max\left[\left(\frac{c_{0\,or\,f(45^\circ)} - c_{0\,or\,f(0^\circ)}}{45^\circ}\right)\alpha_{\sigma_1} + c_{0\,or\,f(0^\circ)};\right.$$
$$\left.\left(\frac{c_{0\,or\,f(90^\circ)} - c_{0\,or\,f(45^\circ)}}{45^\circ}\right)(\alpha_{\sigma_1} - 45^\circ) + c_{0\,or\,f(45^\circ)}\right], \tag{4}$$

where c_0 is the initial cohesion, and c_f is the final cohesion (see Eq. (10)), and α_{σ_1} is the angle between the direction of major principle stress and the normal vector to the bedding plane. The cohesion is assumed to be varied linearly in function of the angle α_{σ_1}, between the cohesion values which are defined for $\alpha_{\sigma_1} = 0^\circ$, $\alpha_{\sigma_1} = 45^\circ$, and $\alpha_{\sigma_1} = 90^\circ$.

The behavior of the solid matrix is considered to be governed by the Terzaghi's postulate with the assumption of a fully water-saturated medium:

$$\sigma'_{ij} = \sigma_{ij} - p_w\delta_{ij}, \tag{5}$$

where σ_{ij} is the total stress tensor, σ'_{ij} is the effective stress tensor, p_w is the pore water pressure, and δ_{ij} is the Kronecker symbol.

The plastic potential surface g is defined as Eq. (6) considering a general non-associated plasticity framework.

$$g \equiv II_{\hat{\sigma}} - m' I_\sigma = 0, \tag{6}$$

with:

$$m' = \frac{2\sin\psi}{\sqrt{3}\,(3 - \sin\psi)}, \tag{7}$$

where ψ is the dilatancy angle. The hardening and/or softening are introduced in this model via an hyperbolic variation of friction angle and/or cohesion (Eqs. (9)-(10)) as a function of Von Mises equivalent plastic strain ε^p_{eq} [18]:

$$\varepsilon^p_{eq} = \int_0^t \sqrt{\frac{2}{3}\left(\dot{\varepsilon}^p_{ij} - \frac{\dot{\varepsilon}^p_v}{3}\delta_{ij}\right)\left(\dot{\varepsilon}^p_{ij} - \frac{\dot{\varepsilon}^p_v}{3}\delta_{ij}\right)}\,\mathrm{d}t, \tag{8}$$

$$\phi_c = \phi_{c0} + \frac{\left(\phi_{cf} - \phi_{c0}\right)\varepsilon^p_{eq}}{B_\phi + \varepsilon^p_{eq}}, \tag{9}$$

$$c = c_0 + \frac{\left(c_f - c_0\right)\varepsilon^p_{eq}}{B_c + \varepsilon^p_{eq}}, \tag{10}$$

where ϕ_{c0} is the initial compression friction angle, ϕ_{cf} is the final compression friction angle, and B_ϕ/B_c are the values of equivalent plastic strain for which half of hardening/softening on friction angle and/or cohesion is achieved.

2.2. Second gradient method

Concerning the numerical computation of localized shear zones in geomaterials, the classical finite element method suffers from a pathological sensitivity to the mesh size in modeling of strain localization [19]. Therefore, a specific approach is needed to overcome this problem in order to properly model the localization phenomenon and post-peak shear strength behavior. To adjust this problem, many investigations have been done in the past proposing different enhanced models incorporated an internal length. A last family of enriched models comes from continua with microstructure which is the case of local second gradient method [20, 21, 22]. This method is used in our coupled hydro-mechanical study as the regularization technique in which the continuum is enriched by the microstructure effects. Thus, the kinematics includes macrokinematics as well as microkinematics [23, 24]. In the framework of microstructure continuum theory, a microkinematic gradient field υ_{ij} is defined to describe strain and rotation at the microscale. With reference to the classical continuum mechanics, additional terms are then added in the internal virtual work of a given body [21].

In the used local second gradient model, it is assumed that microkinematic gradient is equal to the macrodeformation gradient, i.e. $\upsilon_{ij} = F_{ij} = \partial u_i/\partial x_j$. As a result, the virtual microkinematic gradient is also equal to the virtual macrodeformation gradient ($\upsilon^\star_{ij} = F^\star_{ij} = \partial u^\star_i/\partial x_j$). Consequently, the balance equations of the coupled second gradient model in the weak form are obtained following the principle of virtual work as:

$$\int_\Omega\left(\sigma_{ij}\frac{\partial u^\star_i}{\partial x_j} + \Sigma_{ijk}\frac{\partial^2 u^\star_i}{\partial x_j\partial x_k}\right)d\Omega = \int_{\Gamma_\sigma}\left(\bar{t}_i u^\star_i + \overline{T}_i D u^\star_i\right)d\Gamma, \tag{11}$$

$$\int_\Omega\left(\dot{M}p^\star_w - m_i\frac{\partial p^\star_w}{\partial x_i}\right)d\Omega = \int_\Omega Q p^\star_w d\Omega - \int_{\Gamma_q}\overline{q}p^\star_w d\Gamma, \tag{12}$$

where Ω is the current solid configuration (volume), $u^\star_i$ is the virtual displacement field, $\bar{t}_i$ is the external (classical) traction forces per unit area, $\overline{T}_i$ is an additional

external (double) force per unit area that both $\bar{t}_i$ and $\overline{T}_i$ applied on a part Γ_σ of the boundary of Ω, $Du_i^\star$ is the normal derivative of $u_i^\star$, $\dot{M}$ is the time derivative of the water mass inside Ω, $p_w^\star$ is the virtual pore water pressure field, m_i is the mass flow (see Eq. (16)), Q is a sink term, and Γ_q is the part of the boundary where the input water mass per unit area $\overline{q}$ is prescribed. In addition, Σ_{ijk} is the double stress, dual of the virtual (micro) second gradient which needs an additional constitutive law, and it has no link with the pore water pressure. It is defined with an elastic law [20] as a function of (micro) second gradient of the virtual displacement. This second gradient law depends on one elastic parameter D to which the shear band width is proportional [23, 25].

Eqs. (11)-(12) should be solved for every kinematically admissible virtual displacement field $u_i^\star$ and virtual pore water pressure field $p_w^\star$. However, since the second derivative of displacement is demanded for Eq. (11), this Equation needs the use of C^1 function, for the displacement field, to be incorporated into a finite element code. To avoid this procedure, the assumptions $\upsilon_{ij} = F_{ij}$ and $\upsilon_{ij}^\star = F_{ij}^\star$ are introduced through a field of Lagrange multipliers λ_{ij} [23]. Hence, the governing equations of the local second gradient coupled model could be given by:

$$\int_\Omega \left(\sigma_{ij} \frac{\partial u_i^\star}{\partial x_j} + \Sigma_{ijk} \frac{\partial \upsilon_{ij}^\star}{\partial x_k} \right) d\Omega - \int_\Omega \lambda_{ij} \left(\frac{\partial u_i^\star}{\partial x_j} - \upsilon_{ij}^\star \right) d\Omega = \int_{\Gamma_\sigma} \left(\bar{t}_i u_i^\star + \overline{T}_i \upsilon_{ik}^\star n_k \right) d\Gamma, \tag{13}$$

$$\int_\Omega \lambda_{ij}^\star \left(\frac{\partial u_i}{\partial x_j} - \upsilon_{ij} \right) d\Omega = 0, \tag{14}$$

$$\int_\Omega \left(\dot{M} p_w^\star - m_i \frac{\partial p_w^\star}{\partial x_i} \right) d\Omega = \int_\Omega Q p_w^\star d\Omega - \int_{\Gamma_q} \overline{q} p_w^\star d\Gamma, \tag{15}$$

where n_k is the normal vector to the surface Γ_σ. Eqs. (13)-(15) are held for any time t; the virtual quantities in these equations are dependent on the history of boundary conditions and then on the time t.

Using the Darcy's law which governs the water motion relation in an anisotropic porous medium, the water mass flow is given by:

$$m_i = -\rho_w \frac{k_{w,ij}}{\mu_w} \left(\frac{\partial p_w}{\partial x_j} \right); \qquad i, j = 1, 2, \tag{16}$$

where k_w is the intrinsic water permeability, and μ_w is the water dynamic viscosity.

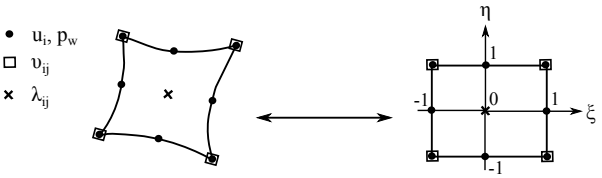

Fig. 1. 2D second gradient finite element: quadrilateral element (left), corresponding parent element (right).

The field equations (13)-(15) are linearized [26] and then they are discretized spatially using 2D plane strain isoparametric finite elements. These elements have eight nodes for the displacement and pore pressure fields (u_i and p_w), four nodes for υ_{ij} and one node for λ_{ij} (see Fig. 1). The quadratic shape functions [27] are applied for the u_i and p_w interpolation whereas the linear shape functions are used for υ_{ij}, and λ_{ij} is supposed to be constant. Readers interested in more details of the coupled finite element scheme may refer to Collin et al. [26].

2.3. Constitutive laws for the contact problem

With regard to the concrete lining of the studied gallery which has been emplaced almost simultaneously with the gallery excavation, the contact mechanism between the clay mass and the lining is an essential issue. The contact is supposed to occur during the gallery excavation while the clay converges towards the lining producing some contact pressure on the interface between two bodies. We propose using the hydro-mechanical interface elements between the Boom clay mass and the concrete lining in order to model their contact phenomenon.

The frictional contact problem are usually treated by mean of elasto-plasticity analogy [28]. A classical elasto-plastic model with the Coulomb yield criterion is used in our study as the mechanical constitutive law for contact behavior (Eq. (17)). We assume that when the contact occurs and two bodies are stuck, this sticking phase is equivalent to the elastic domain of the yield criterion ($f < 0$). Then, the stick and slip states in the contact process would be distinguished by the yield surface ($f = 0$). That is to say when the threshold value in the modulus of the tangential stress is reached, the slip conditions is verified.

$$f = |\tau_T| - \varphi . p'_N, \tag{17}$$

where τ_T is the tangential effective stress, φ is the coulomb friction coefficient, and p'_N is the normal effective stress.

The current case of contact problem is dealing with the sticking phase. The Penalty method has been implemented into Lagamine by Charlier [15] to regularize the sticking contact conditions. Hence, in the case of contact ($p'_N > 0$), a slight penetration of one body into the other and, a tangential relative micro displacement between the contacting bodies could be possibly acceptable. Then, the rate of effective stresses are generally governed by:

$$\begin{bmatrix} \dot{p}'_N \\ \dot{\tau}_T \end{bmatrix} = \begin{bmatrix} -K_N & 0 \\ 0 & K_T \end{bmatrix} \begin{bmatrix} \dot{\varepsilon}_N \\ \dot{\varepsilon}_T \end{bmatrix}, \tag{18}$$

where $\dot{p}'_N$ and $\dot{\tau}_T$ are the rate of normal and tangential components of effective stress, $\dot{\varepsilon}_N$ is the normal relative displacement (interpenetration) velocity, $\dot{\varepsilon}_T$ is the (elastic) tangential micro displacements velocity, and K_N and K_T are the penalty coefficients. Since $\dot{\varepsilon}_N$ takes a negative value in the case of contact and interpenetration of one body into the other, there is a negative sign behind the penalty coefficient K_N in the first relation.
Thence, following this incremental relation, the normal effective stress at the end of a considered time-step during our numerical analysis, called p'^B_N, is given by Eq. 19 while p'^A_N is the corresponding value at the beginning of the time-step.

$$p'^B_N = p'^A_N + \dot{p}'_N.\Delta t \tag{19}$$

where the unilateral condition of the contact problem consists in:

$$p'^B_N = \left\langle p'^B_N \right\rangle \tag{20}$$

where $\langle . \rangle$ are the Macaulay brackets. In fact, in the case of loss of contact, the tensile stress is not admissible, and the normal and tangential components of effective stress (p_N, τ_T) are set equal to zero.

Concerning the hydraulic constitutive law, the fluid flux in the current study is resulting from the transversal exchange between two sides of interface which is technically function of their pressure difference as brought in the following:

$$f^t_w = T^t_w.\Delta p_w.\rho_w, \tag{21}$$

where T^t_w is the transverse transmissivity, p_w is the pore water pressure, and ρ_w is the water density.

Then, with application of these constitutive laws, the 2D isoparametric finite elements with three nodes are used to model the contact problem. These parabolic elements are defined on the interface such that they are compatible (common node and same degree) with the solid finite element used to discretize the corresponding body. Thus, the quadratic interpolation functions [27] are used for displacements and pore pressure fields. Fig. 2 shows schematically the interface element, the two sides in contact are called as structure and foundation here. More details of the finite element framework employed for these elements, their geometrical and algorithmic implementation are beyond the scope of the present paper; they can be found in [15, 18, 29] upon interest.

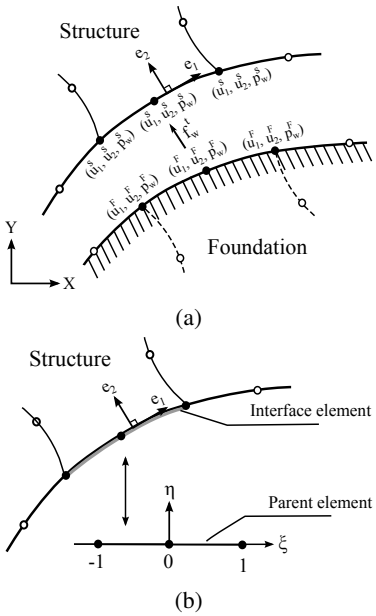

Fig. 2. 2D parabolic interface element (a) discretization description; (e_1, e_2) are the local current basis, and (b) interface element and corresponding parent element.

3. Simulation of EDZ extension through the strain localization approach

The numerical modeling of the shear bands network and extension of EDZ in the large scale gallery excavation in Boom clay host rock is presented in this section through the strain localization approach. Connecting gallery is one of the main galleries excavated in the underground research laboratory, HADES URL, close to the city of Mol (Belgium), in order to study the feasibility of high-level nuclear waste disposal in the Boom Clay layer. Fig. 3 shows a sketch of different galleries including their excavation history in this underground facility, HADES, located at a depth of about 225 m close to the mid-plane of Boom clay formation. The excavation technique chosen for Connecting gallery to

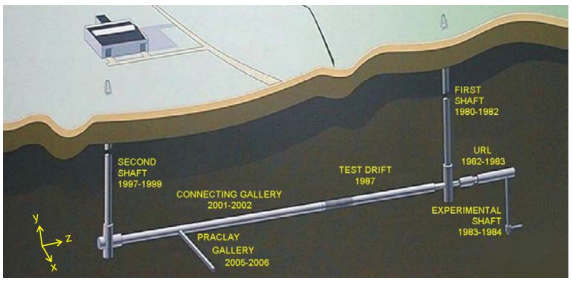

Fig. 3. Sketch of different galleries in HADES for studying the high-level nuclear waste disposal in Boom clay [30].

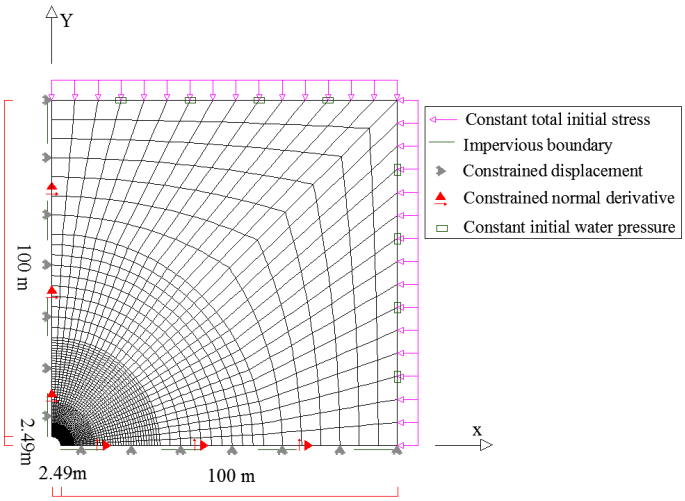

Fig. 4. Geometry of the model.

minimize the extension of the EDZ was using a tunneling machine consisted of a road header under the protection of a shield. In addition, the wedge-block technique has been applied for the gallery's lining. The concrete segments were assembled to form the rings which were then expanded against the excavated clay massif through insertion of one or more key segments. A minimum construction rate of 2 meters per day (between 2-4 meters per day) could be achieved in the steady state [30].

The coupled hydro-mechanical model is intended to reproduce the behavior of the host rock during construction of the gallery and afterwards. A quarter of the gallery is modeled, by assuming symmetry along $x-$ and $y-$axes, using the Finite Element code, Lagamine, from the Université de Liège, taking into account the initial stress anisotropy and material anisotropy. These are able to cause some directional dependency in the clay behavior. Moreover, strain localization can induce a loss of symmetry in the system's response. On the whole, the system may not be basically modeled in the axisymmetric conditions and a plane strain state is considered. In addition, with regard to the latter reason, our modeling is intended to be also extended to a full gallery in order to address the possible influence of strain localization on the symmetrical aspects of the material response, assumed through the primitive modeling of a quarter of the gallery.

One of the most challenging feature about the Connecting gallery, excavated in the plastic Boom clay layer, is the concrete lining of the gallery since it could highly decrease the extension of damaged zone and the convergence around the gallery (see Section 3.4). It must be noted that a simple elastic constitutive law using the total stresses is applied to model the concrete behavior. The important role of this lining as a foundation for the clay mass and the behavior of its interface with the clay during the gallery excavation is an open issue of particular interest which is focused specifically in our study. The latter concerns analyzing the contact mechanism of the lining with Boom clay during the gallery excavation. This phenomenon is discussed in Section 4 by defining the hydro-mechanical interface elements between the lining and the clay. This study is then extended for the modeling of a full gallery.

3.1. Model geometry and properties

Fig. 4 shows the two-dimensional mesh geometry of the model. The gallery has a total excavated radius of 2.49 m taking into account 40 cm of the concrete lining and 9 cm of the gap (over-excavation radius) between the clay mass and the lining. The lining is considered as a continuous structure in stead of the concrete segments with the joints among them [31]. This simplification may more influence the concrete response regarding the relative deformation of the segments, which are not supposed to be critical at the level of the present study. Concerning the over-excavation radius, it is attributed to the total radial displacement (half convergence taking into account the symmetric response) of the clay observed ahead of the excavation front ($45mm$), in the unsupported zone between the rear end of the shield and the installed lining ($10mm$), and at the level of the rear end of the shield ($35mm$) along the gallery axis during the excavation (see [30] if interested). This feature is supposed to be applied implicitly in our 2D plane strain model via a pre-introduced gap between two bodies. During the excavation phase, the clay mass would converge towards the lining while the considered hydro-mechanical interface elements between them can reproduce their contact phenomenon.

The initial boundary conditions are indicated in Fig. 4; the constrained normal derivatives are given to define the symmetry of the radial displacements (u_r) around the symmetric boundaries (i.e. $\partial u_x/\partial y = \upsilon_{12} = 0$ along the x axis and $\partial u_y/\partial x = \upsilon_{21} = 0$ along the y axis). These kinematic boundary conditions are needed to establish correctly the symmetry along $x-$ and $y-$axes, according to Zervos et al. [32]. Indeed, due to the existence of the gradient terms in the equilibrium conditions, the normal derivative of displacements can be also prescribed besides the classical boundary conditions of displacements.

The initial stresses and pore water pressure of the clay mass are defined in the model based on the site measurements. The anisotropic total stresses are applied as $\sigma_{yy} = 4.5MPa$ and $\sigma_{xx} = 3.8475MPa$ ($K_0 = 0.855$) which are decreased to $100kPa$ (atmospheric pressure) on the gallery wall during the excavation phase (6 days) and remain constant until the end of simulation (3.5 years) (see Fig. 5). Furthermore, the initial pore water pressure is equal to $2.25MPa$ followed by a decrease up to the atmospheric pressure on the gallery wall during the excavation phase. Since the convergence of the clay mass due to the excavation is mostly taken place during the excavation phase, it is calculated that the contact between clay and the lining occurs by there. From then on, the water pressure remains constant (equal to the atmospheric pressure) on the internal surface of the concrete lining. It must be noted that the progressive release of the initial stresses and pore water pressure on the gallery wall is introduced in our 2D plane strain model in order to account for 3D impact of the excavation front in its proximity. Moreover, the excavation time interval considered to release the boundary pore pressure is assumed to be the same as the one for the stresses. This choice is based on some site measurements of the pore pressure which have shown the extension of the excavation face impact on the pore water pressure [30]. Thence, taking into account the aforementioned gallery's excavation rate, relative time interval, during which the pore pressure is affected by the excavation front, could be obtained. Although, the excavation time interval for the boundary pore pressure has been considered by some to be different from the one applied for the boundary forces [33].

Given the mechanical constitutive laws described in Section 2, the model parameters are defined in accordance with the hydro-mechanical behavior of Boom clay. Tables 1-3 introduce the mechanical parameters chosen for Boom clay, concrete lining and the interface in our model. The Boom clay properties were investigated in many studies and experimental works

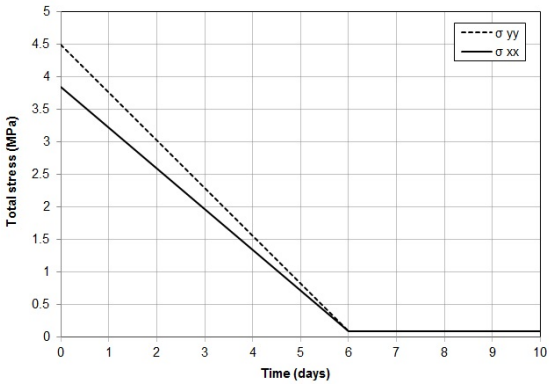

Fig. 5. Imposed total stresses on the gallery wall.

[34, 35, 2, 36] with regard to which the clay parameters have been basically selected in this study. As presented in the former studies of some of the authors [37, 38], this choice could be validated based on some experimental data on Boom clay. Several simulations have been also performed in the framework of parametric study to better define the essential parameters for modeling the strain localization phenomenon in Boom clay layer like cohesion softening (parameters c_f and B_c) [38]. This parametric study confirmed the important role of the cohesion softening for initiating the strain localization in the vicinity of the gallery. Then, the cohesion softening, and friction angle hardening calibrated from the former laboratory triaxial compression tests [36] were introduced to the model. In addition, the zero dilatancy angle - in the range of values proposed in the literature [2] - has been considered since introducing a non-zero dilatancy angle in the model could delay (or, prevent) the onset of strain localization during the excavation phase in the numerical simulation [38], which does seem unrealistic. Moreover, the material anisotropy is considered to model more realistically the response of clay mass to the excavation process accompanied by the onset of localized bands. With this perspective, the anisotropic degree of Young's modulus and initial cohesions were chosen based on the study of François et al. [12] to provide the elastic and plastic cross-anisotropy of the material in Drucker-Prager model implemented in Lagamine. The elastic stiffness matrix considers cross-anisotropy elasticity while the plastic cross-anisotropy is defined by the material cohesion which depends on the angle between major principle stress and the normal to the bedding orientation (see Section 2.1).

The second gradient elastic modulus D is another parameter studied particularly because of its significant effect on modeling of strain localization [39]. The width

Table 1. Boom clay mechanical parameters

Parameter	Symbol	Value	Unit
Young elastic modulus	$E\|\|$	400	MPa
Young elastic modulus	$E\perp$	200	MPa
Poisson ratio	$\vartheta\|\|\|\|$	0.125	-
Poisson ratio	$\vartheta\perp\|\|$	0.0625	-
Shear modulus	$G\perp\|\|$	178	MPa
Initial friction angle	φ_{c0}	8	$^\circ$
Final friction angle	φ_{cf}	18	$^\circ$
Hardening coefficient	B_φ	0.001	-
Initial cohesion	$c_0(0^\circ)$	255	kPa
Initial cohesion	$c_0(45^\circ)$	240	kPa
Initial cohesion	$c_0(90^\circ)$	330	kPa
Final cohesion	$c_f(0^\circ)$	23.18	kPa
Final cohesion	$c_f(45^\circ)$	21.8	kPa
Final cohesion	$c_f(90^\circ)$	30	kPa
Softening coefficient	B_c	0.05	-
Dilatancy angle	Ψ	0	$^\circ$
Second gradient elastic modulus	D	2000	N

Table 2. Concrete mechanical parameters

Parameter	Symbol	Value	Unit
Young elastic modulus	E	43305	MPa
Poisson ratio	ϑ	0.25	-

of the localized shear band is controlled by this constant parameter based on the study of Chambon et al. [23]. The numerical response of the material is therefore mesh independent as it has been demonstrated by Bésuelle et al. [40]. In fact, if some measurements of the band thickness were experimentally performed, the modulus D would be chosen to respect the observed internal length. Moreover, as shown in the latter aforementioned study, the choice of D and the mesh size, in the zone where strain localization takes place, should be consistent so that the numerical requirement of having a minimum of about three elements across the band width is satisfied. Thereby, more refinement of the mesh would increase this number without affecting the results. This sort of recommendation is not only addressed in the used method, but also in any non-local regularization technique. As a result, it can provide a more numerical accuracy in the localization pattern of the solution and post-peak behavior. Within this framework, the second gradient elastic modulus was then chosen equal to $2000N$ based on our parametric study [38, 39].

The hydraulic parameters governing the coupled hydro-mechanical behavior of the clay mass are presented in Table 4 based on the past studies [2]. The anisotropic water permeability [41] is introduced to the model to better capture the coupled phenomenon in Boom clay. Tables 5- 6 lists the hydraulic parameters applied to the model for the concrete lining and the interface.

Table 3. Interface mechanical parameters

Parameter	Symbol	Value	Unit
Penalty coefficient on contact pressure	K_N	3×10^9	N/m^3
Penalty coefficient on contact friction	K_T	3×10^9	N/m^3
Coulomb friction coefficient	φ	0.2	-

Table 4. Boom clay hydraulic parameters

Parameter	Symbol	Value	Unit
Horizontal water permeability	$k_{w,x}$	5.06×10^{-19}	m^2
Vertical water permeability	$k_{w,y}$	2.3×10^{-19}	m^2
Specific mass of water	ρ_w	1×10^3	Kg/m^3
Porosity	ϕ	0.39	-
Water compressibility	$\frac{1}{\chi_w}$	5×10^{-10}	Pa^{-1}
Water dynamic viscosity	μ_w	1×10^{-3}	$Pa.s$
Atmosphere pressure	P_{atm}	1×10^5	Pa

Table 5. Concrete hydraulic parameters

Parameter	Symbol	Value	Unit
Water permeability	k_w	4×10^{-17}	m^2
Porosity	ϕ	0.15	-

Table 6. Interface hydraulic parameters

Parameter	Symbol	Value	Unit
Transverse transmissivity	T^t_w	1×10^{-8}	$m/Pa.s$

3.2. Analysis of the evolution of localized shear bands

Considering the importance of the scale effect in the problems governed by the strain localization and softening [32], numerical analysis of the localization phenomenon during the excavation of a real scale gallery in Boom clay layer is focused in this study. In the following, the results of the modeling are presented. Visualization of the different solutions during the computation is performed by observation of the normalized increment of deviatoric strain, the total deviatoric strain and the plastic loading index in the vicinity of the gallery wall as it is presented in Figs. 6- 8, respectively.

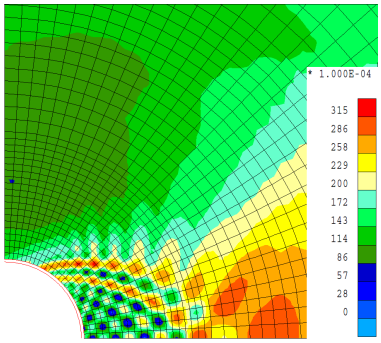

(a)

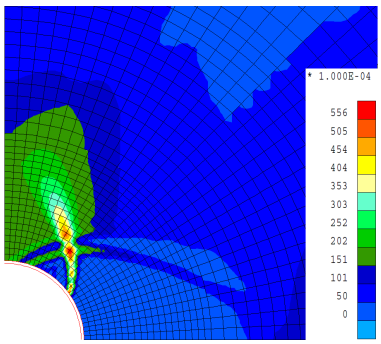

(b)

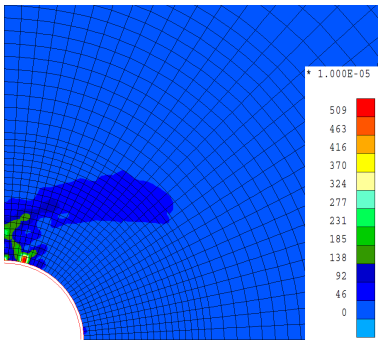

(c)

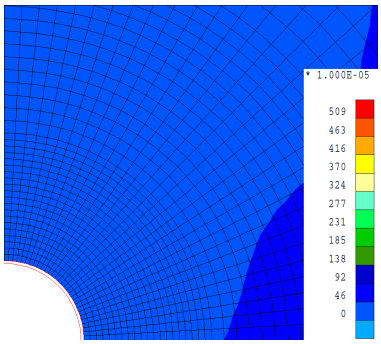

(d)

Fig. 6. Increment of deviatoric strain after (a) 4 days, (b) 5 days, (c) 6 days, and (d) 3.5 years.

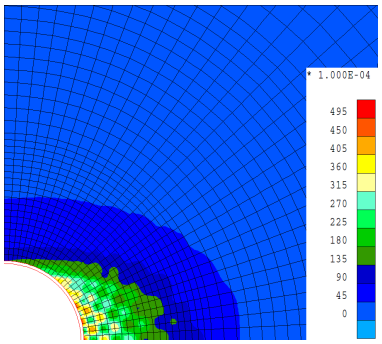

(a)

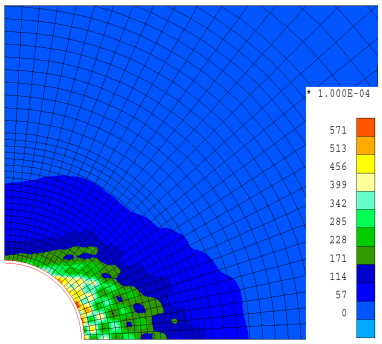

(b)

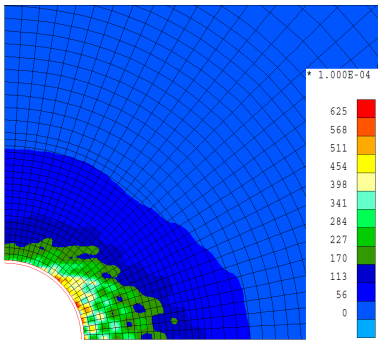

(c)

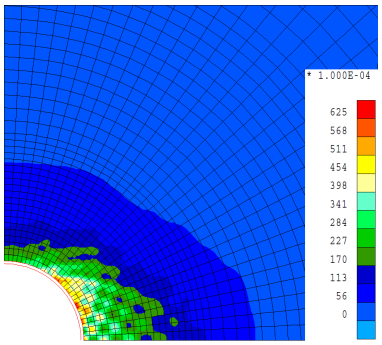

(d)

Fig. 7. Total deviatoric strain after (a) 4 days, (b) 5 days, (c) 6 days, and (d) 3.5 years.

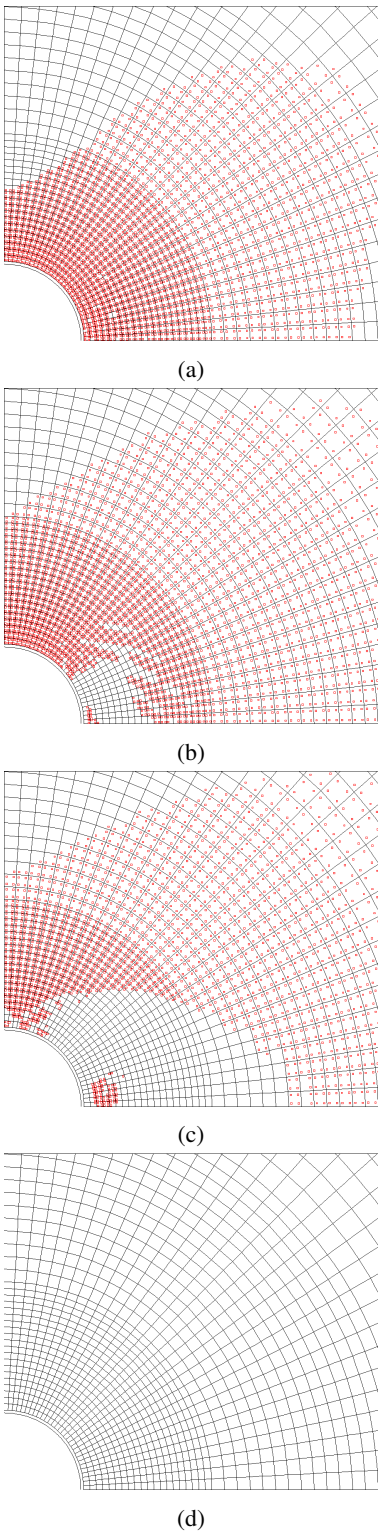

Fig. 8. Plastic loading index after (a) 4 days, (b) 5 days, (c) 6 days, and (d) 3.5 years.

The activity and distribution of the localized shear bands, and their evolutionary appearance and disappearance in different time steps can be observed by the contours of increment of deviatoric strain (Fig. 6). However, the total deviatoric strain in each time step highlights the synthesis of the whole history of the shear bands' activity in the accumulated time (Fig. 7). The latter can underline the total extension of the localized shear bands around the gallery in a considered time. Although, among these localized bands, there are some which may not be currently active. Moreover, the plastic loading index addresses the immediate response of the Gauss points in each element (here there are four Gauss points per element) in terms of the plasticity during the simulation. When a Gauss point undergoes a plastic loading, then a small square is plotted, otherwise, for a Gauss point which undergoes either elastic unloading or reloading, nothing is drawn in the contour (Fig. 8).

The above phenomena are noticeable in Figs. 6- 8 where the evolution of localized shear bands in Boom clay mass, in the radius of $10m$ from the gallery wall, is presented after 4, 5 and 6 days (end of the excavation phase), and 3.5 years (end of the simulation); four significant aspects are observed. First, the onset of localized shear bands is clearly noticed after about 4 days (see Fig. 6a) although this solution is not unique for whole of the excavation time (until 6 days), some of shear bands are not any more active or they are getting less active in the later time steps. Besides, the total deviatoric strain shows an accumulation of the whole activity of the shear bands which occurs mostly during the excavation (see Fig. 7a- 7c). Second, the evolutionary process of the extension of localized zone is quite limited to the excavation period since no considerable activity is observed after excavation: the increment of deviatoric strain does not show any remarkable activity of the shear bands after 6 days (see Fig. 6d). Therefore, the total deviatoric strain at the end of simulation is almost the same as the one at the end of excavation (compare Figs. 7c and 7d). Third, plastic loading index (Fig. 8) indicates the appearance of plasticity at the excavation time which is followed by the elastic unloading at some Gauss points giving birth to the localized bands (see Fig. 8b); i.e. there is possibly an elastic unloading outside of the localized bands. This plasticity index corresponds to the response observed in the current time step similarly to the normalized increment of deviatoric strain. Hence, the current activity of the localized shear bands is quite reflected on the plastic points in each time step. Forth, the loss of symmetry observed in the clay response is induced by three definite phenomena: ma-

terial anisotropy - cohesion depending on the angle between major principle stress and the normal to the bedding orientation, cross-anisotropy of the elastic properties, and anisotropy of the hydraulic conductivity - the anisotropic initial stress, and non-symmetric pattern of strain localization process. The latter which is also depending on the post-peak behavior and cohesion softening characteristics within the shear bands prompts the non-symmetric orientation of the shear bands with regard to the hydro-mechanical response of the clay mass and lining.

On the whole, the total deviatoric strain after the end of excavation phase can be a reference of the extension of localized zone (the shear bands don't have any distinguished activity afterwards). Thus, the eye-shape (anisotropic) extension of the Excavation Damaged Zone (EDZ) around the Connecting gallery can be estimated as about 2.8m horizontally and 0.6m vertically.

3.3. Numerical modeling compared to the in-situ observations

The fracturing pattern observations around the Connecting gallery consists of two main conjugated shear planes. These fracture planes are dipped crossing the mid-height of the gallery. Further away from the gallery axis, they are curved at their intersection with the vertical and horizontal planes passing through the gallery axis, although this curve was found to be more accentuated vertically than horizontally [30]. Therefore, the vertical extension of EDZ with respect to the gallery axis is less than the horizontal one, with respect to which the results of our numerical simulation are consistent so far. Fig. 9 presents schematically the fracturing pattern observed around the Connecting gallery during its construction. The observation along a vertical cross-section parallel to the gallery axis (in the y-z plane with reference to the sketch brought in Fig. 3) shows that radial extension of less than one meter or more precisely 0.6m [9] was identified in the vertical direction, which confirms the numerical prediction.

Besides the in-situ evidence of an eye-shape extension of the EDZ around the gallery (Fig. 9b) which can justify our numerical prediction (see Fig. 7d, and Fig. 18), the similar pattern has been observed in the small-scale laboratory experiments as well [42].

During the excavation of the Connecting gallery, the radial convergence of the clay in the unsupported zone between the rear end of the shield and the installed lining was observed to be higher in the horizontal direction (parallel to bedding)) than the vertical one (perpendicular to bedding). In fact, the horizontal diameter seemed

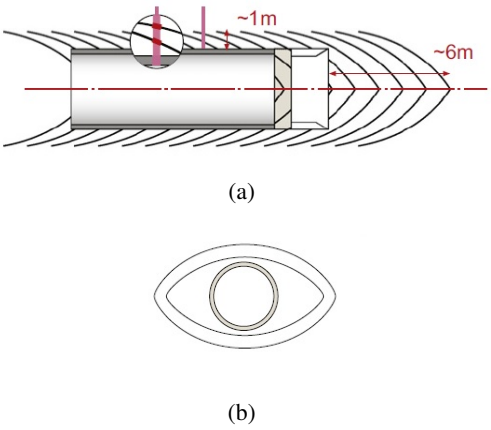

Fig. 9. Schematic representation of the fracturing pattern observed along a (a) vertical cross-section parallel to the gallery axis, (b) a cross-section perpendicular to the gallery axis [2].

to be small to emplace the key segments of the lining although the vertical diameter was large enough. Consequently, a trimming of the clay sidewalls ($10-20mm$) was even necessary over a portion of the gallery before placing the lining [9, 30]. This anisotropic convergence of the clay sidewalls is also noticed in our numerical simulations. Fig. 10 presents the radial displacement (or, half convergence under the assumption of a symmetric response) of the clay after the simulated excavation phase (i.e. 6 days) for two studied node (in the horizontal and vertical directions) along the gallery wall. As it is observed, the total horizontal displacement is more than the vertical one. Moreover, a maximum deformation of about 10mm is estimated for the lining in the horizontal direction - upon contact with the clay - with respect to 90mm of the initial gap considered between the clay and the lining in the numerical simulation (see Section 3.1). This 10mm of the horizontal displacement over the considered over-excavation radius is identified in an equivalent manner as the trimming of the clay sidewall evidenced during the gallery's construction. On the contrary, similarly to the in-situ observations, Fig. 10 shows that the total vertical displacement is less than the over-excavation radius (90mm).

3.4. Role of the concrete lining

The gallery excavation in Boom clay as a plastic clay can result in a relatively high convergence [43]. Therefore, the concrete lining of the excavated underground galleries has an essential role in order to decrease the convergence of the host rock around the gallery wall. In addition, thanks to the lining, the extension of the damaged zone around the gallery is also effectively reduced

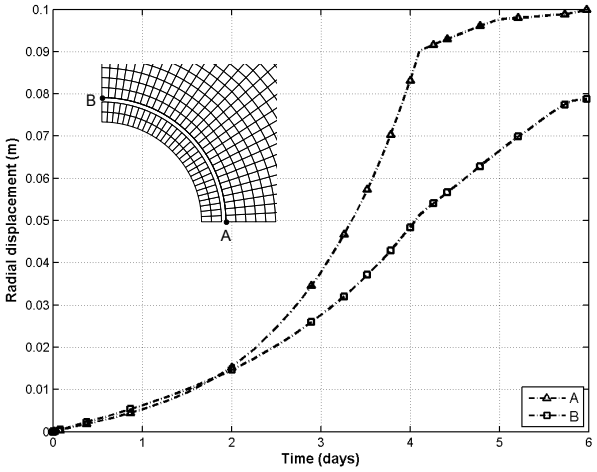

Fig. 10. Horizontal and vertical displacement of the clay sidewalls after 6 days.

consequently to the contact between the clay and the lining initiated during the excavation. This phenomenon is accompanied by the contact pressure developed on the interface between these two bodies. The latter will be more discussed in the next section.

To better clarify the significant influence of the lining, the numerical simulation of the extension of the localized zone around the Connecting gallery, excavated in Boom clay formation, without the concrete lining is presented here. The similar initial boundary conditions as the real gallery case (i.e. with the lining) has been applied to the model. Figs. 11- 13 show the evolution of localized shear bands within the clay in the radius of 20m around the studied gallery without the lining. The results are brought in terms of the increment of deviatoric strain (Fig. 11), total deviatoric strain (Fig. 12) and plastic loading index (Fig. 13) after 4, 5 and 6 days (end of the excavation phase), and 3.5 years (end of the simulation). The study shows that the shear bands are still active even some years after the end of excavation (see Figs. 11d and 13d). In fact, the evolution of the total deviatoric strain and consequently, the extension of the damaged zone are considerable at the end of simulation compared to the end of excavation. (compare Figs. 12c and 12d). Hence, the estimated anisotropic extension of the localized shear bands around the gallery without the lining is about 16m horizontally and 4.4m vertically. This is averagely more than 6.5 times of the EDZ predicted around the gallery with the concrete lining (Section 3.2), which was consistent with the in-situ observation (see Section 3.3). Moreover, as a consequence of this high extension of the damaged zone, the total radial displacement of the clay sidewalls is about

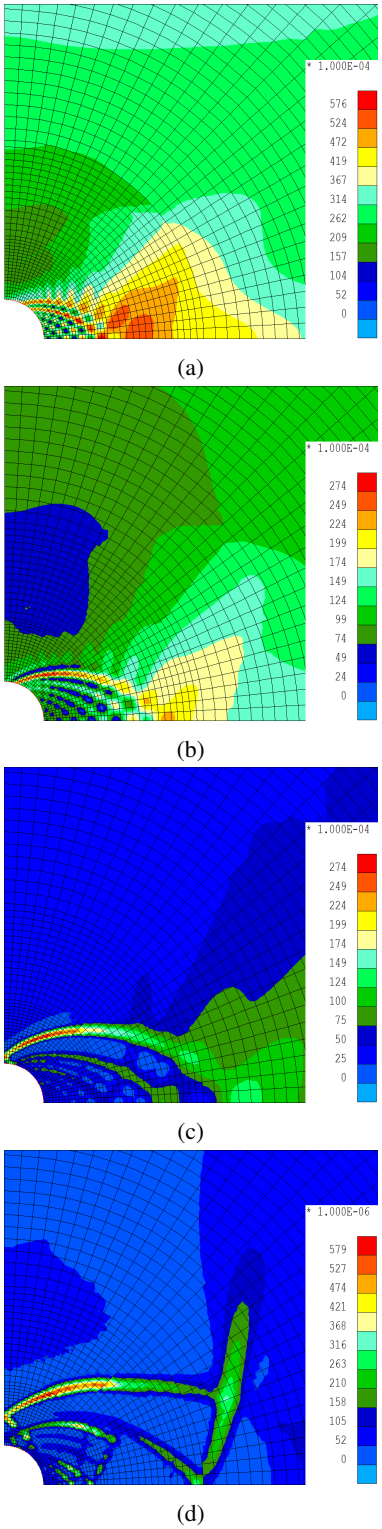

(a)

(b)

(c)

(d)

Fig. 11. Increment of deviatoric strain around the gallery without the concrete lining after (a) 4 days, (b) 5 days, (c) 6 days, and (d) 3.5 years.

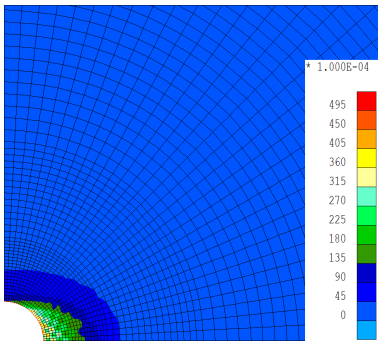

(a)

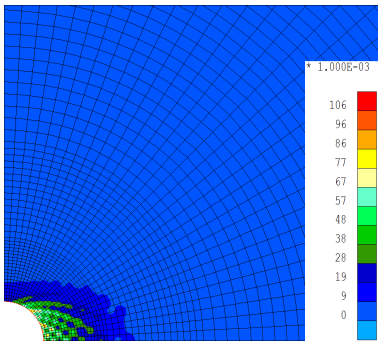

(b)

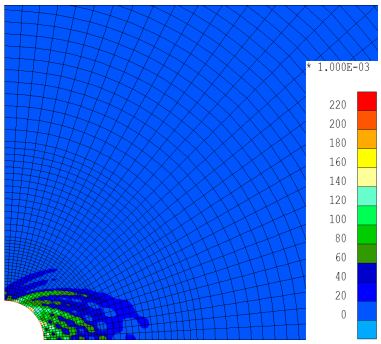

(c)

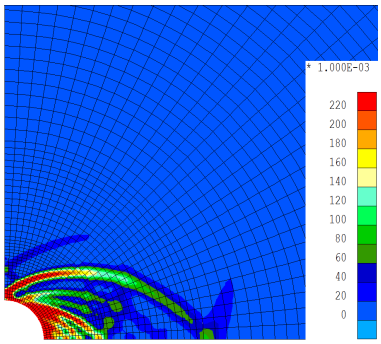

(d)

Fig. 12. Total deviatoric strain around the gallery without the concrete lining after (a) 4 days, (b) 5 days, (c) 6 days, and (d) 3.5 years.

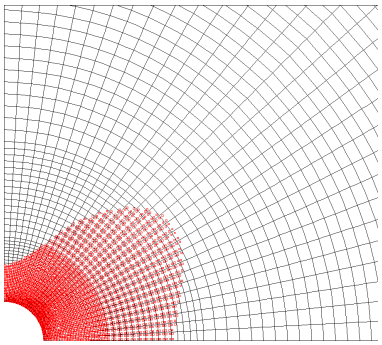

(a)

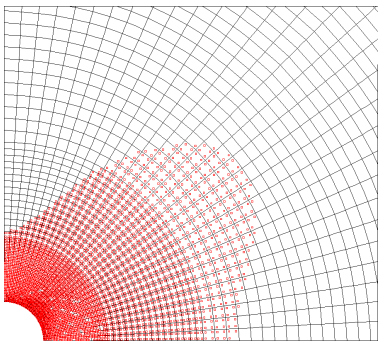

(b)

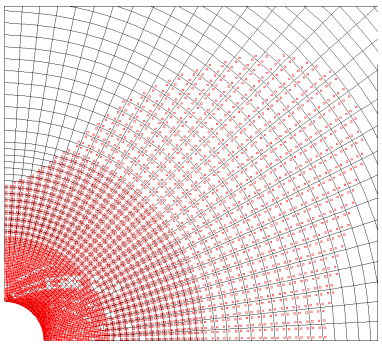

(c)

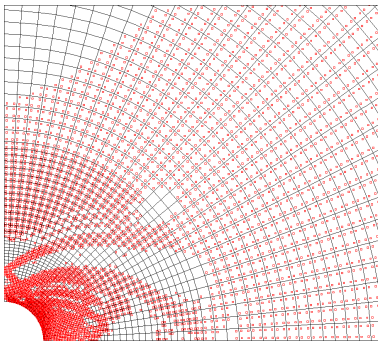

(d)

Fig. 13. Plastic loading index around the gallery without the concrete lining after (a) 4 days, (b) 5 days, (c) 6 days, and (d) 3.5 years.

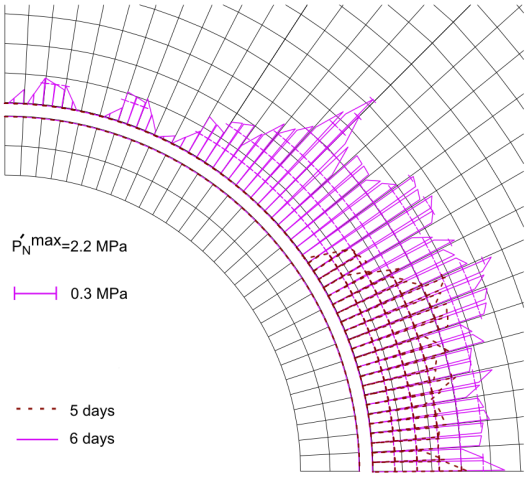

Fig. 14. Diagram of the normal contact pressure on the interface.

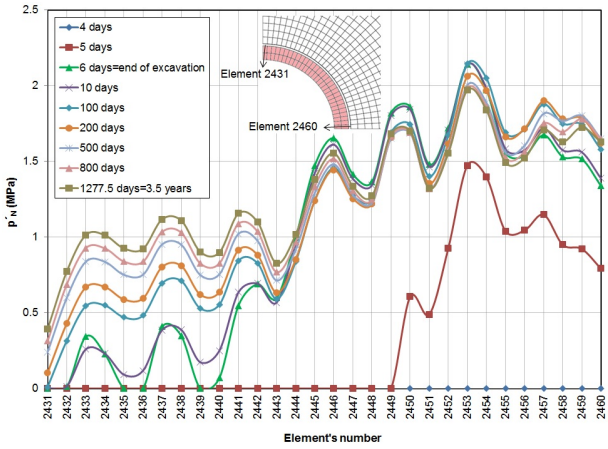

Fig. 15. The development of the normal contact pressure on the interface.

0.9m horizontally and 0.6m vertically that is considerably increased compared to the case of gallery with the lining (Section 3.3).

4. Analysis of the contact pressure on the interface

The coupled contact process between the clay mass and the concrete lining simultaneously with the gallery excavation and onset of the localized shear bands, and in the long-term is an open crucial topic which needs to be analyzed. The contact occurs during the excavation time inducing the contact pressure on the interface between two bodies. From then on, it does not allow important evolution of shear bands around the gallery in the clay mass. Thus, it can have an essential impact on the reduction of EDZ.

Fig. 14 shows the diagram of the normal contact pressure on the interface between the lining of Connecting gallery and Boom clay mass after 5 days and 6 days (i.e end of excavation). As it is observed, the contact is initiated on the horizontal side and then, it is developed on the whole interface until the end of excavation. This phenomenon confirms the anisotropic response of the clay during the excavation as it was discussed in Section 3.2. In fact, due to the ovalization pattern in deformation of the clay mass during the excavation, the bottom elements firstly come in contact with the lining and normal contact pressure is established on the interface.

The normal contact pressure on the interface elements (on the first integration point of each element; there are two integration points per element) throughout the excavation phase and afterwards is brought in Fig. 15 to better clarify the pressure's time-dependent evolution process. The maximum of contact pressure is primarily taken place on the interface bottom side during the excavation which can induce a left-side horizontal movement of the lining as well. Consequently, there is an upward vertical movement of the lining. The clay mass and lining are tended to behave oppositely in long-term which prompts the increase of contact pressure on the top elements of interface throughout the time after the end of excavation.

Moreover, some oscillations are observed in the evolution pattern of normal contact pressure on the interface. The oscillatory type of response has been studied to find out any possible numerical or physical origin. Our theory is that the physical aspect gives birth to these oscillations. That is to say the evolution pattern of the localized shear bands around the gallery (see Section 3.2). In fact, the oscillation of normal contact pressure on the interface is comparatively related to the shear bands created around the gallery. Fig. 16 shows superposition of the normal contact pressure on the interface (Fig. 14) and the total deviatoric strain in Boom clay mass around the gallery (Figs. 7b-7c) during the excavation. An essential accordance is noticed between these two phenomena. Indeed, the larger shear bands are reasonably compared with the peaks of the contact pressure produced on the interface. Furthermore, the both features affirm the anisotropic pattern of the clay response.

In addition to the basic physical origin of the observed oscillations, there are generally several numerical characteristics which might also induce this kind of oscillations, based on the literature. The number of integration points considered for the interface elements and the applied numerical integration scheme

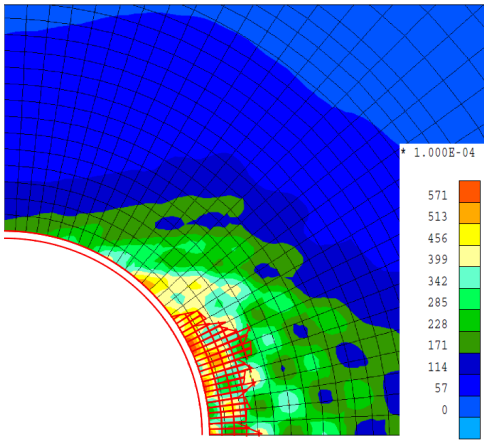

(a)

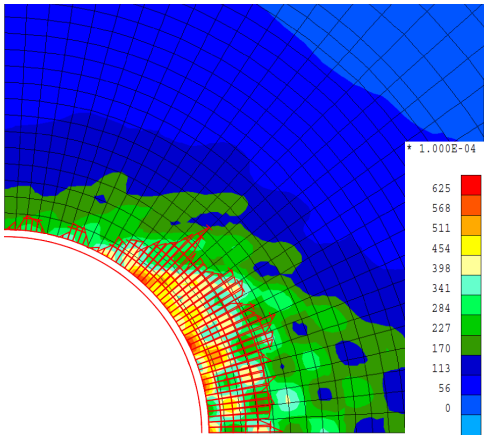

(b)

Fig. 16. Superposition of the localized shear bands and normal contact pressure on the interface after, (a) 5 days, (b) 6 days.

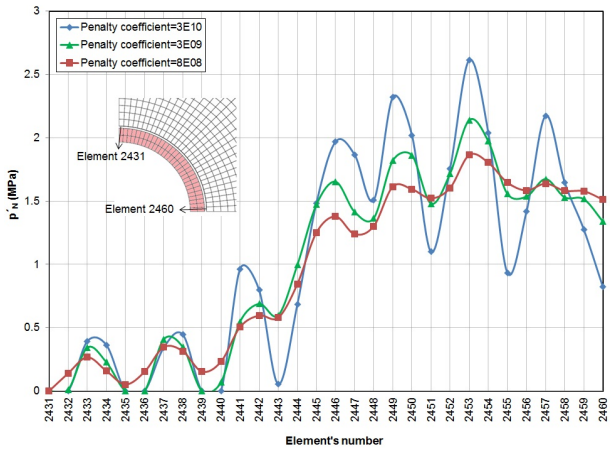

Fig. 17. The influence of penalty coefficient on development of the normal contact pressure on the interface.

may have some impacts on the oscillatory form of response [44]. However, several simulations performed in our study with the application of different numerical approach (Newton-Cotes, Lobatto, and Gauss integration schemes; the latter is our fundamental scheme) have shown that the number of integration points and the applied numerical integration scheme cannot improve the observed oscillations in our numerical case. Furthermore, the penalty coefficient introduced into the model is another candidate to be fairly responsible for the observed response. Practically, this coefficient should be defined big enough (compared to the rigidity of solid) in order to limit the interpenetration of the two bodies in contact [15]. Nevertheless, increasing of this coefficient has some limitations since it may generally result in some numerical convergence troubles and ill-conditioned system. It may be noteworthy to declare that in this study, convergence criteria for the displacements and forces are governed by:

$$\mathfrak{Conve}_D = \sqrt{\frac{1}{N_{Anal}} \sum_{1}^{N_{Anal}} \left(\frac{\sum_{N_{Dof}} [\delta \mathfrak{u}]^2}{\sum_{N_{Dof}} [\Delta \mathfrak{u}]^2} \right)} \leq \mathfrak{Tol}_D \tag{22}$$

$$\mathfrak{Conve}_F = \sqrt{\frac{1}{N_{Anal}} \sum_{1}^{N_{Anal}} \left(\frac{\sum_{N_{Dof}} F_{OBF}^2}{\sum_{N_{Dof}} N_{OBF}} \Big/ \frac{\sum_{N_{Dof}} F_{REA}^2}{\sum_{N_{Dof}} N_{REA}} \right)} \leq \mathfrak{Tol}_F \tag{23}$$

where $\delta \mathfrak{u}$ is the increment of displacement - which refers to the mechanical displacements, pore pressure variations and the change in second gradient terms - between the current and previous iterations, $\Delta \mathfrak{u}$ is the displacement occurred between the current iteration and the end of previous step, F_{OBF} is the out-of-balance force, F_{REA} is the reaction force, N_{OBF} and N_{REA} are the number of out-of-balance forces and reactions corresponding to each degree of freedom, N_{Dof} is the number of degrees of freedom, N_{Anal} is the number of facet types involved in our analysis; i.e. three in our case: mechanical (displacements), hydraulic (pore pressure), and second gradient terms, and $\mathfrak{Tol}_D/\mathfrak{Tol}_F$ are the input tolerance parameters; it is defined as 1×10^{-3} in our model. The (time) step then converges if $\mathfrak{Conve}_D$ and $\mathfrak{Conve}_F$ are satisfied.

Therefore, the penalty coefficient should be carefully introduced in the model in order to satisfy the convergence criterion while the interpenetration of two bodies in contact is also possibly minimized. Our study showed that this coefficient has an impact on the oscillatory pattern of contact pressure on the interface. See Fig. 17 for the development of the normal contact pressure on the interface with the application of three different penalty coefficients ($3 \times 10^9\ N/m^3$ has been basically defined in our modelings as it was brought in Table 3). Decreasing the penalty coefficient by one order of magnitude could fairly reduce the amplitude of the pressure's oscillation produced on the interface. However, more reduction could not make an important change in the observed oscillations, and it can rather increase the interpenetration of two bodies in contact. On the other hand, by increasing the penalty coefficient after a limit (around $3 \times 10^9\ N/m^3$ in our case), there is a considerable negative influence on the amplitude of pressures' oscillations produced on the interface; besides, there may be sort of numerical convergence restriction as well. It is noteworthy that the applied penalty method to regularize the contact problem in the present paper can be compared with another regularization technique developed by [45] with a particular focus on the unsaturated flow in porous medium. On the whole, the value given to the penalty coefficient so far seems convenient and as yet, it has partially reduced the oscillations' amplitude. However, from a fundamental point of view, these oscillations have been identified to result from the evolution pattern of the localized shear bands around the gallery independent of the applied numerical approach.

To ensure that aforesaid phenomena are true for the modeling of a full gallery, the latter's result is presented in Fig. 18. It shows the extension of the localized shear bands at the end of excavation (6 days) with reference to the total deviatoric strain, superposed by the normal contact pressure on the interface. In terms of the strain localization, an eye-shape extension of the EDZ has been being expected to be created around the gallery with respect to what has been already observed for a quarter of the gallery (see Section 3.2), and this is noticed in Fig. 18. All at once, a general quasi-symmetric pattern is observed with regard to the model of a quarter of the gallery (Fig. 16b). However, a totally full symmetrical response of the system is not necessarily expected when the strain localization plays an important role in the modeling [46]. Hence, some non-symmetric aspects are supposed to be observed in the development of normal contact pressure on the interface where there is a loss of symmetry in the pattern of localized shear bands within the surrounding clay (i.e. mostly in the vertical direction in our case). This results from the physical relation between the structure of normal contact pressure on the interface and the localized shear bands around the gallery.

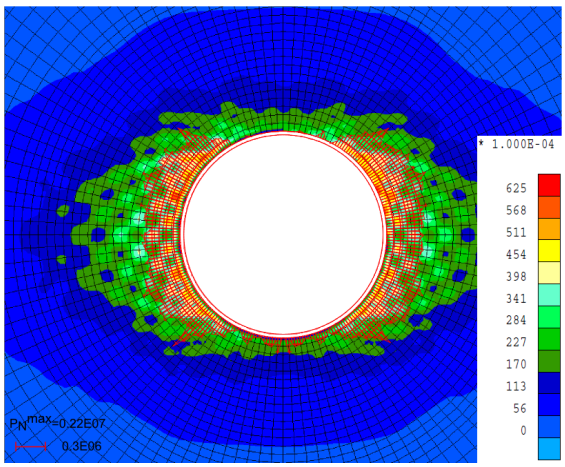

Fig. 18. Superposition of the localized shear bands and normal contact pressure on the interface after 6 days: The modeling of a full gallery.

5. Pore water pressure evolution around the gallery

This part of the study reveals some hydraulic aspect of the coupled hydro-mechanical analysis of Boom clay behavior during the excavation of Connecting gallery, and afterwards. Fig. 19 shows the evolution of pore water pressure for three cross-sections - horizontal, inclined (45°) and vertical - in function of the distance from the gallery wall, and for different time steps during the simulation. The results are presented for a total radius of 100 meters around the gallery, in addition to a close-up of the results in the vicinity of the gallery wall.

Pore water pressure is tended to be stabilized approaching its initial value by getting far from the gallery because of the less influence of excavation process. Moreover, a local increase of pore pressure is observed near to the gallery wall along the horizontal cross-section, specially shortly after the excavation phase. On the contrary, a local decrease of pore pressure is noticed along the vertical cross-section. It must be noted that the material remains still in the saturated state even though some negative pore pressure is attained in the vertical proximity of the gallery. The latter is due to the quite high air entry value defined for Boom clay in our model (3 MPa), based on some available experimental results [36].

The influence of the hydro-mechanical coupled response could make an accumulation of pore pressure

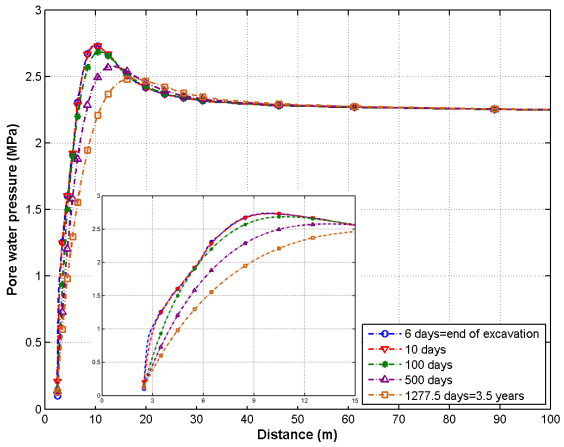

(a)

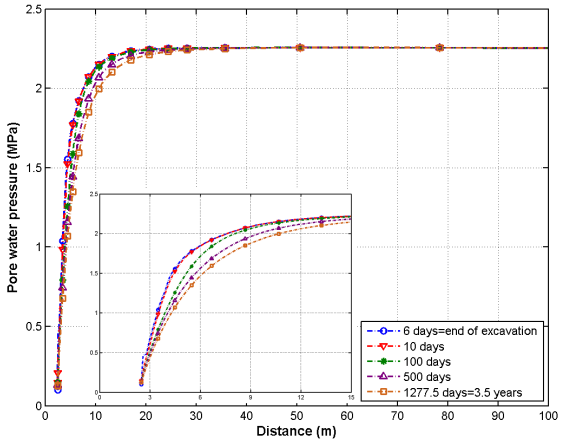

(b)

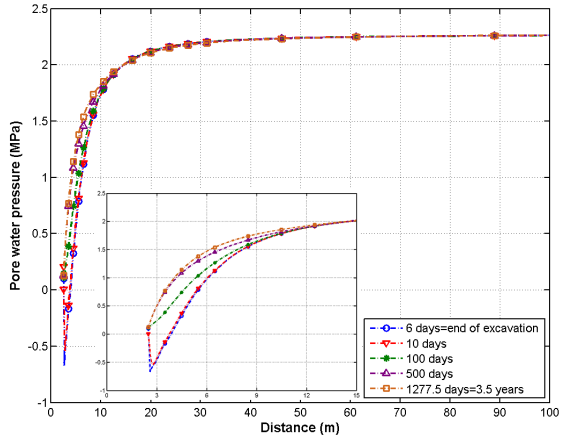

(c)

Fig. 19. Pore water pressure evolution along (a) horizontal, (b) inclined (45°), and (c) vertical cross-sections.

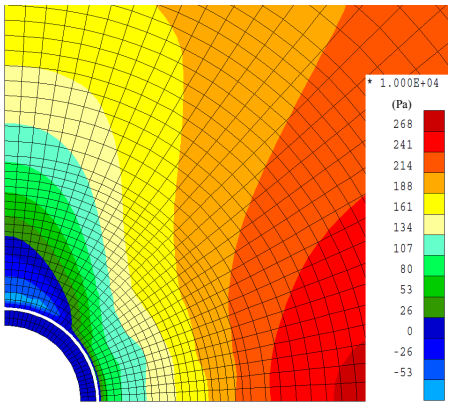

Fig. 20. Contour of pore water pressure around the gallery at the end of excavation (6 days).

along the horizontal direction where the most accentuated localized shear bands appear during the excavation. In fact, pore pressure's evolution is consistent with the mechanical ovalized deformation of the host rock due to the excavation. Consequently to the contact mechanism which is first initiated on the horizontal side (see Section 4), the horizontal displacement of the rock is restricted and such global decrease of pore pressure in the gallery's proximity - which could be caused by excavation - is not observed. In addition, an immediate undrained hydraulic response of the clay also influences the pattern of pore water pressure variations around the gallery. In the long term, these phenomena could be followed by an internal water flow conducted from the vertical side towards the horizontal axis. The contour of the pore water pressure in the vicinity of the gallery at the end of excavation (i.e. 6 days) is shown in Fig. 20.

Furthermore, the impact of localized bands could be slightly noticed through the instantaneous evolution of the pore water pressure upon the excavation, in the form of some small fluctuations (see Fig. 19a), similarly to the results presented in some former studies [39, 47, 48].

6. Conclusions

The creation of an Excavation Damaged Zone is an inevitable outcome of the gallery excavation in the deep geological formation. Given the importance of this issue in the framework of disposal of high-level nuclear waste, the coupled hydro-mechanical behavior of Boom clay, as one of the potential host rocks for this purpose, has been investigated. This paper has firstly presented the extension of the fractures' network and localized shear bands due to the excavation of Connect-

ing gallery (HADES URL, Mol, Belgium) in Boom clay host rock. To do this, a finite element approach was used into which an elasto-plastic model with the Drucker-Prager yield surface in conjunction with the second gradient method have been incorporated. The gallery contains a concrete lining which is being in contact with the soil during the excavation phase. Then, the interface elements has been proposed in order to model the coupled contact phenomenon on the interface between two bodies and the relative response of Boom clay. Using the proposed approach, the formation and evolution of shear zones within the clay mass were reliably simulated and the development of normal contact pressure on the interface between the lining and the massive was well characterized. The numerical prediction of the fracturing pattern and extension of the localized shear bands within the clay around the gallery is in a good agreement with the in-situ observations. Furthermore, the significant role of the gallery's lining has been highlighted in decreasing the convergence of the clay and thus, the extension of damaged zone around the gallery.

The progressive development of contact pressure on the lining generated since the excavation time was analyzed with a particular focus on the origin of the observed oscillations in its evolution pattern. The effect of localized shear bands was fundamentally recognized as the basis of these oscillations as well as partial influence of the numerical penalty coefficient on the amplitude of the oscillations.

The evolution of pore water pressure within Boom clay around the gallery has been analyzed during the excavation and afterwards. The hydro-mechanical coupled response could be noticed by the pore water pressure development in the vicinity of the gallery. Indeed, the latter is consistent with the mechanical anisotropic convergence and shearing pattern. Thence, a local increase of pore pressure is tended, in the gallery's proximity, along the horizontal direction on the contrary to the vertical one.

Acknowledgement

The authors would like to thank the Belgian National Agency for Radioactive Waste and enriched Fissile Material, ONDRAF/NIRAS, for their financial support in this study. This work is part of the first author's Ph.D. thesis.

References

[1] Chapman N, Hooper A. The disposal of radioactive wastes underground. Proceedings of the Geologists' Association 2012;123(1):46 – 63.

[2] Bernier F, Li XL, Bastiaens W. Twenty-five years' geotechnical observation and testing in the tertiary Boom clay formation. Géotechnique 2007;57(2):229–37.

[3] Tsang CF, Bernier F, Davies C. Geohydromechanical processes in the excavation damaged zone in crystalline rock, rock salt, and indurated and plastic clays—in the context of radioactive waste disposal. International Journal of Rock Mechanics and Mining Sciences 2005;42(1):109–25.

[4] Tsang CF, Barnichon JD, Birkholzer J, Li XL, Liu HH, Sillen X. Coupled thermo-hydro-mechanical processes in the near field of a high-level radioactive waste repository in clay formations. International Journal of Rock Mechanics and Mining Sciences 2012;49:31–44.

[5] Bastiaens W, Bernier F, Li XL. Selfrac: Experiments and conclusions on fracturing, self-healing and self-sealing processes in clays. Physics and Chemistry of the Earth, Parts A/B/C 2007;32(8–14):600 –15. Clay in natural and engineered barriers for radioactive waste confinement - Part 2.

[6] Bésuelle P, Viggiani G, Desrues J, Coll C, Charrier P. A laboratory experimental study of the hydromechanical behavior of Boom clay. Rock Mechanics and Rock Engineering 2014;47(1):143–55.

[7] Lenoir N, Bornert M, Desrues J, Bésuelle P, Viggiani G. Volumetric digital image correlation applied to x-ray microtomography images from triaxial compression tests on argillaceous rock. Strain 2007;43(3):193–205.

[8] Desrues J, Viggiani G. Strain localization in sand: an overview of the experimental results obtained in grenoble using stereophotogrammetry. International Journal for Numerical and Analytical Methods in Geomechanics 2004;28(4):279–321.

[9] Mertens J, Bastiaens W, Dehandschutter B. Characterisation of induced discontinuities in the Boom clay around the underground excavations (urf, mol, belgium). Applied clay science 2004;26(1):413–28.

[10] Callari C. Coupled numerical analysis of strain localization induced by shallow tunnels in saturated soils. Computers and Geotechnics 2004;31(3):193–207.

[11] Callari C, Armero F, Abati A. Strong discontinuities in partially saturated poroplastic solids. Computer Methods in Applied Mechanics and Engineering 2010;199(23):1513–35.

[12] François B, Labiouse V, Dizier A, Marinelli F, Charlier R, Collin F. Hollow cylinder tests on Boom clay: Modelling of strain localization in the anisotropic excavation damaged zone. Rock mechanics and rock engineering 2012;47(1):71–86.

[13] Gawin D, Baggio P, Schrefler BA. Coupled heat, water and gas flow in deformable porous media. International Journal for numerical methods in fluids 1995;20(8-9):969–87.

[14] Collin F, Li XL, Radu JP, Charlier R. Thermo-hydro-mechanical coupling in clay barriers. Engineering Geology 2002;64(2–3):179 –93. Key Issues in Waste Isolation Research.

[15] Charlier R. Approche unifiée de quelques problèmes non linéaires de mécanique des milieux continus par la méthode des éléments fini. Ph.D. thesis; Université de Liège; 1987.

[16] Collin F. Couplages thermo-hydro-mécaniques dans les sols et les roches tendres partiellement saturés. Ph.D. thesis; Université de Liège; 2003.

[17] Drucker DC, Prager W. Soil mechanics and plastic analysis or limit design. Quarterly of applied mathematics 1952;10(2):157–65.

[18] Barnichon JD. Finite element modelling in structural and petroleum geology. Ph.D. thesis; Université de Liège; 1998.

[19] Collin F, Levasseur S, Chambon R. Numerical post failure methods in multiphysical problems. European Journal of Environmental and Civil Engineering 2009;13(7-8):983–1004.

[20] Mindlin R. Micro-structure in linear elasticity. Archive for Ra-

tional Mechanics and Analysis 1964;16(1):51–78.
[21] Germain P. The method of virtual power in continuum mechanics. part 2: Microstructure. SIAM Journal on Applied Mathematics 1973;25(3):556–75.
[22] Rice JR. The localization of plastic deformation. Division of Engineering, Brown University; 1976.
[23] Chambon R, Caillerie D, El Hassan N. One-dimensional localisation studied with a second grade model. European Journal of Mechanics-A/Solids 1998;17(4):637–56.
[24] Chambon R, Caillerie D, Matsuchima T. Plastic continuum with microstructure, local second gradient theories for geomaterials: localization studies. International Journal of Solids and Structures 2001;38(46):8503–27.
[25] Kotronis P, Collin F, Bésuelle P, Chambon R, Mazars J. Local second gradient models and damage mechanics: 1d post-localization studies in concrete specimens. In: Bifurcations, Instabilities, Degradation in Geomechanics. Springer; 2007, p. 127–42.
[26] Collin F, Chambon R, Charlier R. A finite element method for poro mechanical modelling of geotechnical problems using local second gradient models. International journal for numerical methods in engineering 2006;65(11):1749–72.
[27] Zienkiewicz OC, Taylor RL. The finite element method: Solid mechanics; vol. 2. Butterworth-heinemann; 2000.
[28] Curnier A. A theory of friction. International Journal of Solids and Structures 1984;20(7):637–47.
[29] Cerfontaine B, Dieudonné AC, Radu JP, Collin F, Charlier R. 3D zero-thickness coupled interface finite element: Formulation and application. Computers and Geotechnics 2015;69:124–40.
[30] Bastiaens W, Bernier F, Buyens M, Demarche M, Li XL, Linotte JM, et al. Euridice report: The connecting gallery. Tech. Rep.; EIG EURIDICE; 2003.
[31] Working Group No. 2 , International Tunnelling Association , et al. Guidelines for the design of shield tunnel lining. Tunnelling and Underground Space Technology 2000;15(3):303–31.
[32] Zervos A, Papanastasiou P, Vardoulakis I. Modelling of localisation and scale effect in thick-walled cylinders with gradient elastoplasticity. International Journal of Solids and Structures 2001;38(30):5081–95.
[33] Callari C, Casini S. Tunnels in saturated elasto-plastic soils: three-dimensional validation of a plane simulation procedure. In: Mechanical Modelling and Computational Issues in Civil Engineering. Springer; 2005, p. 143–64.
[34] SCK-CEN . HADES TOUR GUIDE. Notebook; 1997.
[35] ONDRAF/NIRAS . Technical overview of the safir 2 report: Safety assessment and feasibility interim report 2. Tech. Rep. NIROND 2001–05 E; 2001.
[36] TIMODAZ . THM characterisation and input for simulation. Tech. Rep. WP 3.1, D5; Commision of the Europeen Communities; 2010. Editor: Delage, P.
[37] Dizier A. Caractérisation des effets de températures dans la zone endommagée autour de tunnel de stockage de déchets nucléaires dans des roches argileuses. Ph.D. thesis; 2011.
[38] Salehnia F. Geomechanics applied to nuclear waste disposal; strain localization in Boom clay. Tech. Rep.; Université de Liège; 2013. Annual report to ONDRAF/NIRAS.
[39] Salehnia F, Charlier R, Levasseur S. Modeling of strain localization around the radioactive waste disposal galleries. In: Coupled Phenomena in Environmental Geotechnics. CRC Press; 2013, p. 443.
[40] Bésuelle P, Chambon R, Collin F. Switching deformation modes in post-localization solutions with a quasibrittle material. Journal of Mechanics of materials and structures 2006;1(7):1115–34.
[41] Wemaere I, Marivoet J, Labat S. Hydraulic conductivity variability of the Boom clay in north-east belgium based on four core drilled boreholes. Physics and Chemistry of the Earth, Parts A/B/C 2008;33:S24–36.
[42] Labiouse V, Sauthier C, You S. Hollow cylinder simulation experiments of galleries in Boom clay formation. Rock Mechanics and Rock Engineering 2013;47(1):43–55.
[43] Van Marcke P, Bastiaens W. Excavation induced fractures in a plastic clay formation: Observations at the hades urf. Journal of Structural Geology 2010;32(11):1677–84.
[44] Schellekens JCJ, De Borst R. On the numerical integration of interface elements. International Journal for Numerical Methods in Engineering 1993;36(1):43–66.
[45] Abati A, Callari C. Finite element formulation of unilateral boundary conditions for unsaturated flow in porous continua. Water Resources Research 2014;50(6):5114–30.
[46] Sieffert Y, A-l Holo S, Chambon R. Loss of uniqueness of numerical solutions of the borehole problem modelled with enhanced media. International Journal of Solids and Structures 2009;46(17):3173–97.
[47] Pardoen B, Levasseur S, Collin F. Using local second gradient model and shear strain localisation to model the excavation damaged zone in unsaturated claystone. Rock Mechanics and Rock Engineering 2014;:1–24.
[48] Salehnia F, Charlier R, Sillen X, Dizier A. Modeling of excavation damaged zone through the strain localization approach in Boom clay. In: Computer methods and recent advances in geomechanics. CRC Press; 2014, p. 335.